Precision Spectroscopy of Negative-Ion Resonances in Ultralong-Range Rydberg Molecules

F. Engel,[1] T. Dieterle,[1] F. Hummel,[2] C. Fey,[2] P. Schmelcher,[2,3] R. Löw,[1] T. Pfau,[1] and F. Meinert[1]
[1]5. Physikalisches Institut and Center for Integrated Quantum Science and Technology, Universität Stuttgart, Pfaffenwaldring 57, 70569 Stuttgart, Germany
[2]Zentrum für optische Quantentechnologien, Fachbereich Physik, Universität Hamburg, 22761 Hamburg, Germany
[3]The Hamburg Centre for Ultrafast Imaging, Universität Hamburg, 22761 Hamburg, Germany

(Received 17 April 2019; published 16 August 2019)

The level structure of negative ions near the electron detachment limit dictates the low-energy scattering of an electron with the parent neutral atom. We demonstrate that a single ultracold atom bound inside a Rydberg orbit forming an ultralong-range Rydberg molecule provides an atomic-scale system that is highly sensitive to electron-neutral scattering and thus allows for detailed insights into the underlying near-threshold anion states. Our measurements reveal the so-far unobserved fine structure of the ^3P_J triplet of Rb^- and allows us to extract parameters of the associated p-wave scattering resonances that deviate from previous theoretical estimates. Moreover, we observe a novel alignment mechanism for Rydberg molecules mediated by spin-orbit coupling in the negative ion.

DOI: 10.1103/PhysRevLett.123.073003

Negative ions constitute remarkable objects that have been studied intensively over the past decades [1,2]. In contrast to neutral atoms or positively charged ions, anions are much more weakly bound by shallow and short-range potentials and typically feature only few bound states. As a consequence, they have been proven ideal model systems for investigating the role of electron-electron correlations on their level structure [2]. More recently, the observation of excited opposite-parity bound states [3] has triggered renewed interest in high-resolution negative-ion spectroscopy [4–6] motivated by prospects to realize laser cooling for trapped anions [7,8].

The fine details of the interaction potentials that determine negative-ion bound states also dictate the very low-energy quantum scattering of their neutral parent atom with a free electron [9–11]. Particularly, broad scattering resonances can arise when the associated negative-ion system hosts a short-lived transient state, bound by a centrifugal barrier and located just a few meV above the electron detachment limit. Accessing details of these underlying anion states such as relativistic fine-structure effects experimentally, however, is challenged by their short lifetime, low energy [12], or by selection rules in photodetachment studies starting from the negative-ion ground state [13]. In this Letter, we demonstrate a completely different route to investigate these systems by devising an ultrasensitive microscopic scattering laboratory provided by an ultralong-range Rydberg molecule (ULRM) [14–17]. ULRMs consist of a Rydberg atom that binds to a neutral ground-state atom inside the electron orbit via frequent low-energy scattering of the latter with the quasifree Rydberg electron.

Here, we exploit ULRMs at an unprecedented quantitative level and demonstrate their potential to perform precise spectroscopy of negative-ion resonances at the example of the quasibound ^3P_J state of Rb^-. To this end, we identify previously unobserved molecular states, which are dominated by resonant electron-atom p-wave scattering, and thereby allow us to reveal the presence of relativistic spin-orbit coupling leading to a fine-structure triplet ($J \in \{0, 1, 2\}$). The latter was predicted theoretically for the heavy alkali metals Rb^-, Cs^-, and Fr^-, but so far remained experimentally inaccessible [10,18]. Moreover, we observe that the presence of spin-orbit interaction aligns the ULRM even for spherically symmetric Rydberg S states [19]. Our approach holds intriguing perspectives for high-resolution probing of more complex perturbers such as molecules or clusters [20,21].

An ULRM naturally provides a highly adjustable atomic-scale system for precise studies of electron-neutral scattering at collisions energies in the meV regime [16,22]. Apart from the capability to achieve very low scattering energies unfeasible to realize with free electrons, the high precision arises from the resonating Rydberg electron wave confined in the Coulomb potential, and the resulting narrow Rydberg states. Consider now the presence of a single neutral ground-state atom inside the Rydberg orbit at a distance R from the Rydberg core. Quantum scattering of the electron off the perturber gives rise to a phase shift imparted on the electron wave function, which is detectable via a slight shift of the Rydberg electron resonance energy.

Here, we focus on ultralong-range dimers consisting of a single ^{87}Rb ground-state atom inside the orbit of $nS_{1/2}$ Rb

Rydberg states ($n = 31, \ldots, 37$). For values of R comparable to the size of the Rydberg orbit, the semiclassical electron momentum k is sufficiently small so that s-wave scattering, as quantified by an energy-dependent (triplet) scattering length $a_s^T(k)$, dominates. This gives rise to a smoothly varying potential energy of the system as a function of R that reflects the nodal structure of the Rydberg electron wave function (see Fig. 1) [14,15,23]. For smaller values of R the electron momentum increases and p-wave scattering can become relevant. Importantly, the p-wave contribution is enhanced by a shape resonance arising from the presence of the $Rb^-(^3P)$ state [24,25], which *ab initio* theoretical predictions locate about 23 meV above the Rb-e^- threshold [10,18]. The resonant p-wave contribution leads to deep potential energy minima with decreasing R when the electron kinetic energy approaches the ^3P resonance. The motion of the perturber atom is dictated by the resulting potential energy curve (PEC) and quantized due to the strong radial confinement associated with the potential wells, leading to discrete vibrational dimer states. In Fig. 1, the resulting lowest lying vibrational wave functions are indicated for the s-wave (p-wave) dominated wells at $R = 1450a_0$ ($R = 890a_0$).

Let us now turn to the internal spin structure of the system and in particular the consequence of spin-orbit coupling in the $Rb^-(^3P_J)$ state. In general, the latter gives rise to three (overlapping) anion states and consequently to a splitting of the single shape resonance into a triplet. A theoretical treatment of this spin-orbit coupling in the context of ULRMs has been provided in Refs. [15,26,27]. For the PEC in Fig. 1, the spin-orbit interaction leads to a splitting of the deep p-wave dominated potential well into three substates, while the s-wave dominated outer part of the PEC is essentially unaffected. The splitting is due to three different p-wave scattering channels associated with the (^3P_J) states, which are quantified by respective (triplet) scattering lengths $a_{p,J}^T(k)$. Each of the three split PECs is twofold degenerate and can be associated with a different projection of the total angular momentum on the internuclear axis $|\Omega| = |m_F + m_j|$ [26]. Here, m_j and m_F denote magnetic quantum numbers for the Rydberg electron spin and the ground-state atom hyperfine level, respectively. We focus on the experimentally relevant PECs for $F = 2$.

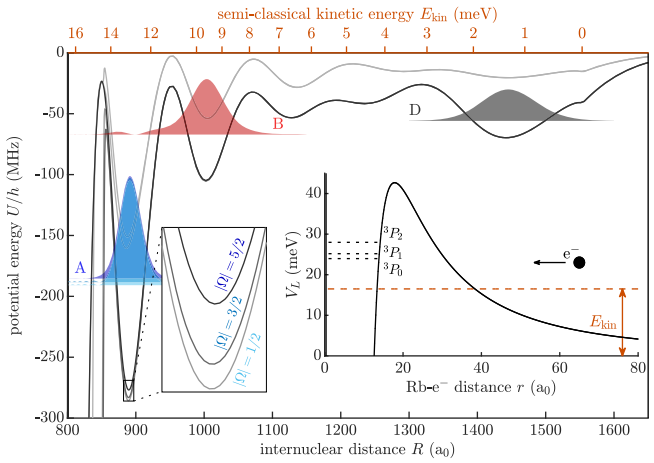

FIG. 1. Anion spectroscopy in ULRMs. Molecular potential energy for the $31S$ Rydberg level owing to (triplet) Rb-e^- scattering as a function of internuclear distance R (black line). Vibrational wave functions for the molecular states A (blue), B (red), and D (black) are denoted by shaded areas. The p-wave dominated well ($R = 890a_0$) is split due to the Rb^- fine-structure triplet ^3P_J. For completeness, the gray line shows the shallow PEC originating from mixed singlet-triplet scattering (not accessed in this work). Inset: Long-range centrifugal barrier leading to the ^3P_J states (dotted lines) of Rb^- above the electron detachment limit ($V_L = 0$).

According to the above considerations, the potential detection of spin-orbit interaction in the (^3P_J) negative-ion system requires investigation of deeply bound dimer states with sufficient resonant p-wave scattering character. In a first set of experiments, we aim to identify and study these candidates via extensive molecular spectroscopy. To this end, we perform Rydberg spectroscopy incorporating field ionization and subsequent ion detection starting from an ultracold (1.5 μK) ensemble of typically 4.5×10^6 ^{87}Rb atoms prepared in the fully spin-stretched $|F = 2, m_F = 2\rangle$ hyperfine state and held in a magnetic quadrupole trap. In the trap, the atoms experience a homogeneous magnetic offset field set to $B = 2.2$ G. We address $nS_{1/2}$ Rydberg states via two-photon spectroscopy involving the intermediate $6P_{3/2}$ state at typical intermediate detunings between $+80$ and $+400$ MHz, and laser polarizations set to address the Zeeman sublevel $m_j = 1/2$.

An exemplary spectrum of the ULRMs below the $|35S_{1/2}, m_j = 1/2; F = 2, m_F = 2\rangle$ asymptote is shown in Fig. 2(a). The strongest molecular line at -22.6 MHz corresponds to the s-wave dominated dimer (D) [16]. Additional lines with smaller binding energy are excited dimers bound by quantum reflection [28], previously studied in [22]. For larger binding energies, we observe two comparatively broad and so-far unexplored resonances labeled A and B, which we attribute to the two deeply bound dimer states depicted in Fig. 1 for $n = 31$. Four remaining resonances are attributed to trimer states with binding energies that match the sum of dimer lines [22]. Specifically, these comprise the simplest trimer formed by two atoms in the s-wave dimer state (T), a trimer formed by one atom in the s-wave dimer and one in the dimer state B ($B + D$), as well as trimers formed when one perturber resides in the strongest excited dimer state ($B + D^*$ and $D + D^*$).

In order to investigate the role of spin-orbit coupling on the deeply bound dimer A, we have taken spectra as shown in Fig. 2(a) for a range of principal quantum numbers. The measured binding energies for the states D, A, and B are

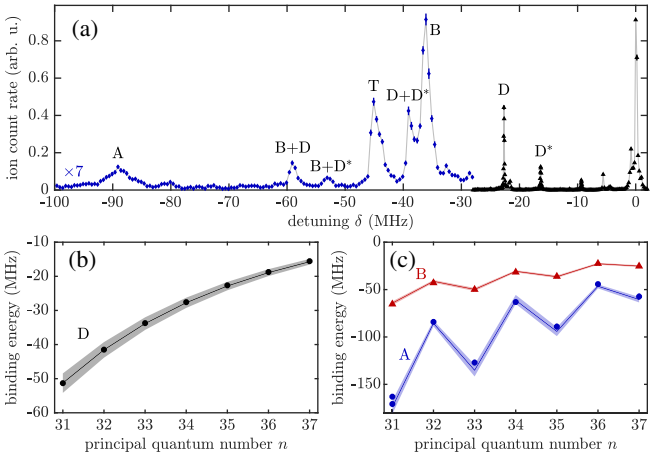

FIG. 2. ULRM spectroscopy for extracting s- and p-wave scattering lengths. (a) Ion signal as a function of detuning δ from the atomic Rydberg line $|35S_{1/2}, m_j = 1/2\rangle$. Deeply bound molecular states are magnified for better visibility. Solid lines connect the data points to guide the eye. (b) Binding energy of the outermost dimer D as a function of n. (c) Binding energies of the deeply bound dimers A (circles) and B (triangles) as a function of n. Solid lines show results from a Green's function calculation with fitted s- and p-wave scattering lengths (see the text). The shaded areas mark small variations on the scattering lengths as described in the text. Error bars in (a) and all other spectra denote one standard deviation. Error bars for the measured binding energies in (b) and (c) are smaller than the data points.

depicted in Figs. 2(b) and 2(c). For the s-wave dominated dimer, we observe the well-known monotonic decrease of the binding energy with n [16]. The deeply bound states A and B, however, show a qualitatively different behavior characterized by a strong alternation of their energy with n. Note that state B appears as a single resonance for all n. The same holds for state A except for $n = 31$. Here, we observe a doublet structure split by $\approx$8 MHz.

In a next step, we perform numerical simulations based on a Fermi model, which allow us to extract triplet s- and p-wave scattering lengths from our data. To this end, we combine advantages from two different methods for simulating PECs, i.e., Green's function calculus and Hamiltonian diagonalization on a finite basis set. Briefly, the Green's function approach intrinsically provides converged results accounting for all Rydberg levels but lacks the possibility to include the full molecular spin structure [15]. Full diagonalization allows us to include all relevant spin degrees of freedom [26,27,39], but exhibits uncertainties originating from the chosen size of the basis set [40]. We stress that it is the combination of both methods that permits conclusions on a precise quantitative level by adapting the employed basis set as outlined in the following.

The starting point is the comparatively simple spin configuration investigated in our experiment, i.e., ULRMs associated with the $|35S_{1/2}, m_j = 1/2; F = 2, m_F = 2\rangle$ asymptote. For negligible spin-orbit interaction, these molecules are described by a single (triplet) s- and p-wave scattering channel [22]. Importantly, in that case complications due to atomic hyperfine structure or Rydberg fine structure do not play a role [41,42]. The PEC and the associated vibrational molecular states are then obtained from Green's function calculations. First, we have computed the molecular states D, A, and B using s- and p-wave scattering length data from *ab initio* calculations [10,18] and found rather poor agreement with the data in Fig. 2(c), particularly for the p-wave dominated state A. Second, we adapted the s- and p-wave scattering lengths [$a_s^T(k)$ and $a_p^T(k)$] that enter the calculations, aiming for improved agreement between experiment and simulation results. For this, we employ a comparatively simple model potential to compute the k-dependent scattering lengths, consisting of a long-range polarization potential and a short-range adjustable hard wall [27,28,43]. Moreover, note that the s- and p-wave channel can be adjusted independently by exploiting that the binding energy of the s-wave dominated dimer (D) is essentially unaffected by the p-wave channel.

The molecular binding energies computed with the adjusted scattering lengths are depicted with solid lines in Figs. 2(b) and 2(c). We obtain a zero-energy s-wave scattering length $a_s^T(0) = -15.2a_0$ and a value for the p-wave shape-resonance position $E_r^{\mathrm{avg}} = 26.6$ meV [44]. In order to estimate uncertainties for these values, the range of binding energies obtained from slight changes of the scattering lengths is indicated by shaded regions. Those correspond to variations in $a_s^T(0)$ of $\pm 0.5a_0$ and E_r^{avg} of ± 0.2 meV. Note that the (J-averaged) resonance position predicted in Ref. [10] based on a two active-electron model to account for electron correlations is about 20% smaller. Similar discrepancy has been found in photodetachment experiments of Cs^- [10,13]. For $a_s^T(0)$, the obtained value lies between previous theoretical estimates ($-13a_0$ [10], $-16.9a_0$ [45]).

While the Green's function calculation allows us to predict the observed molecular binding energies, it does not explain the measured doublet structure of the p-wave dominated state A for $n = 31$. In the following, we investigate this state in more detail and demonstrate that the level splitting is directly related to the fine structure of the ^3P_J negative-ion resonance. High-resolution spectroscopy of the observed doublet is shown in Fig. 3 for three increasing values of the magnetic field B. We observe a strong qualitative change in the spectral shape when changing the magnetic field from about 2 to 15 G. While the doublet is observed for comparatively small fields (triangles), a single resonance modulated by a characteristic narrow substructure appears for higher values of B (diamonds).

To explain this observation, we now include the full molecular spin structure into our calculation of PECs via diagonalization of the system Hamiltonian on a finite basis set [26–28]. Here, the fine structure of the anion enters the computation via three J-dependent p-wave scattering

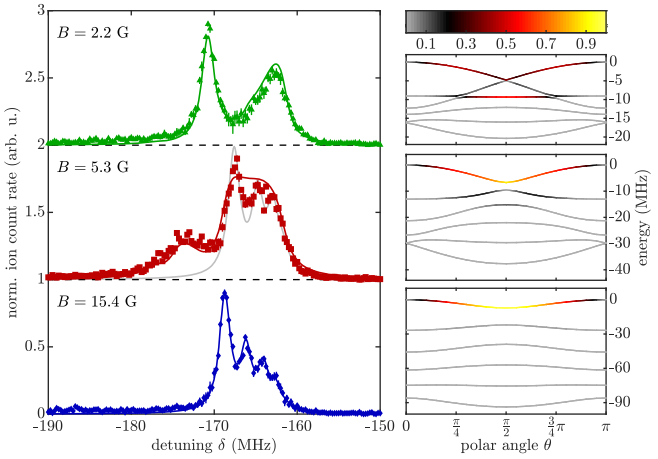

FIG. 3. Spin-orbit interaction and molecular alignment. (Left) Spectra of the p-wave dominated molecular state A with $n = 31$ and for magnetic fields B as indicated. Zero detuning corresponds to the atomic Rydberg line $|31S_{1/2}, m_j = 1/2\rangle$. Solid lines are simulated line shapes based on the θ-dependent PECs [28]. (Right) Angular dependence of the PECs evaluated at the minimum of the potential well in which state A is localized ($R = 890a_0$). Energies are referenced to the maximum of the uppermost PEC. The three plots are computed for the magnetic field present in the corresponding measurement, i.e., for increasing values of B from top to bottom. Coloring encodes the projection onto $m_j = 1/2$ and $m_F = 2$ (see the text).

channels, quantified by their corresponding scattering lengths $a^T_{p,J}(k)$. We calculate the scattering lengths using the short-range parameters obtained above from the data in Fig. 2, but now add standard LS interaction to our model potential [28], which delivers the J-dependent $a^T_{p,J}(k)$ and the corresponding shape-resonance positions E^J_r. Evidently, our approach yields values for E^J_r that fulfil Landé's interval rule, as expected for pure Russel-Sounders coupling [10]. Importantly, we can largely reduce the aforementioned uncertainties arising from the choice of the basis set by switching off the anion fine structure in the calculation and then adapting the basis set to match the previous Green's function results, yielding four hydrogenic Rydberg manifolds with $n-5$ to $n-2$ [28].

While the PECs shown in Fig. 1 are computed for a field-free situation, the magnetic field present in the experiment renders the situation even richer. Specifically, the Zeeman energy of the electron spins lifts the pairwise degeneracy of the three $|\Omega|$ states. Furthermore, when the effect of spin orbit coupling is sufficiently strong, the PECs obtain additional angular dependence as a result of an angular-dependent mixing of the three p-wave scattering channels [19]. Computed PECs for the values of B set in the experiment are shown in Fig. 3 (right column). For $B = 2.2$ G, our laser excitation scheme couples only to the upper two PECs as indicated by the coloring, which denotes the absolute square of the projection of the electronic molecular state onto $|m_j = 1/2; F = 2, m_F = 2\rangle$ weighted by the solid angle $\sin(\theta)$. Note that for negligible spin-orbit interaction, the PECs are independent of θ and one only couples to the highest energy state ($\Omega = +5/2$). The observed doublet is thus a direct consequence of the ${}^3P_J$ fine structure.

With increasing B the Zeeman shift separates the θ-dependent PECs and only the curve with $\Omega = +5/2$ can be addressed. Moreover, the increasing angular confinement finally aligns the molecule, leading to a series of discrete pendular states. This transition from a doublet to a single relevant PEC that exhibits a pendular-state substructure (Fig. 3, $B = 15.4$ G) is in excellent agreement with the experimental observation. For a quantitative comparison, the spectra are compared to simulated line shapes using a semiclassical sampling approach based on the relevant PECs in the case of unresolved pendular states ($B = 2.2$ G and $B = 5.3$ G) and a rigid-rotor model when individual pendular states are observed ($B = 15.4$ G) [28]. Deviations for $B = 5.3$ G in the spectral part associated with the uppermost PEC are due to the onset of strong molecular alignment, as seen by comparison to the rigid-rotor model prediction based on that PEC (gray line). Moreover, the excellent agreement between theory and experiment allows for extracting the fine-structure splitting of the ${}^3P_J$ anion state [28]. For the fitted results shown in Fig. 3, we obtain $E_r^{J=(0,1,2)} = (24.4, 25.5, 27.7)$ meV, respectively. Apart from the systematically larger value of the measured E_r^{avg}

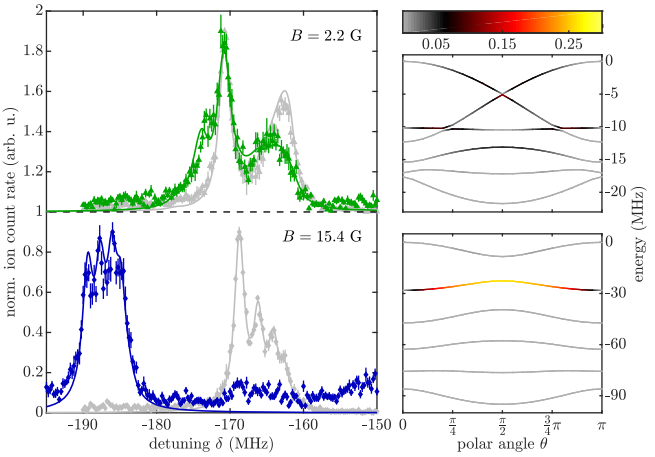

FIG. 4. Spin character of the spin-orbit affected ULRM. (Left) Spectra of the p-wave dominated molecular state A for $n = 31$ with laser polarization set to address the $m_j = -1/2$ atomic Rydberg state and for magnetic fields B as indicated. Gray data sets show the corresponding spectra for $m_j = 1/2$ reprinted from Fig. 3 for comparison. Zero detuning corresponds to the atomic Rydberg line $|31S_{1/2}, m_j = 1/2\rangle$. Solid lines are simulated line shapes based on the θ-dependent PECs. (Right) Angular dependence of the corresponding PECs similar to the ones shown in Fig. 3. Coloring now encodes the projection onto $m_j = -1/2$ and $m_F = 2$.

discussed above, the obtained fine-structure splitting is in good agreement with the predictions in Ref. [10].

Finally, we investigate the spin character of the PECs in the presence of spin-orbit coupling by changing the laser polarization to couple to the $|31S_{1/2}, m_j = -1/2\rangle$ Rydberg level. Measured spectra of the molecular state A are shown in Fig. 4 for two different settings of the magnetic field. For the low-field data ($B = 2.2$ G) the spectrum only slightly changes due to a small shift of the excitation strength to smaller energies. Note that this is again an effect of spin-orbit interaction, which strongly mixes the spin character of the θ-dependent PECs. For larger values of B, this spin mixing is less pronounced and our excitation scheme mostly couples to the second highest energy state ($\Omega = +3/2$). This is reflected in the experiment data for $B = 15.4$ G, showing a pronounced Zeeman shift of resolved pendular states. Again, we find excellent agreement with simulated line shapes.

In conclusion, we have exploited ULRMs for precise measurements on a quasibound negative-ion resonance. A careful analysis of measured binding energies allowed us to extract s- and p-wave scattering lengths and pinpoint the positions of the p-wave shape resonances associated with the ^3P_J fine-structure triplet of Rb^-. We expect that the obtained scattering data will form the basis for future experiments on evermore delicate aspects of ULRMs, comprising few-body effects [46,47], molecular dynamics, or more complex spin couplings [41]. These prospects also call for developing Green's function calculations including all molecular spins. Moverover, our results allow for refining sophisticated predictions for low-energy electron-neutral scattering [10,15,18]. The presented technique for measuring fine details of near-threshold negative-ion resonances can further be transferred to benchmark other atomic and potentially also molecular systems featuring intriguing low-energy scattering properties [11,48,49].

We thank M. Eiles for numerous discussions and W. Li for assistance with the Green's function calculations. We acknowledge support from Deutsche Forschungsgemeinschaft [Grants No. PF 381/13-1, No. PF 381/17-1, and No. SCHM 885/30-1, the latter two being part of the SPP 1929 (GiRyd)]. F. M. acknowledges support from the Carl-Zeiss Foundation and is indebted to the Baden-Württemberg-Stiftung for the financial support by the Eliteprogramm for Postdocs.

[1] T. Andersen, Phys. Rep. **394**, 157 (2004).
[2] D. J. Pegg, Rep. Prog. Phys. **67**, 857 (2004).
[3] R. C. Bilodeau and H. K. Haugen, Phys. Rev. Lett. **85**, 534 (2000).
[4] U. Warring, M. Amoretti, C. Canali, A. Fischer, R. Heyne, J. O. Meier, Ch. Morhard, and A. Kellerbauer, Phys. Rev. Lett. **102**, 043001 (2009).
[5] C. W. Walter, N. D. Gibson, D. J. Matyas, C. Crocker, K. A. Dungan, B. R. Matola, and J. Rohlén, Phys. Rev. Lett. **113**, 063001 (2014).
[6] E. Jordan, G. Cerchiari, S. Fritzsche, and A. Kellerbauer, Phys. Rev. Lett. **115**, 113001 (2015).
[7] A. Kellerbauer and J. Walz, New J. Phys. **8**, 45 (2006).
[8] L. Pan and D. R. Beck, Phys. Rev. A **82**, 014501 (2010).
[9] S. J. Buckman and C. W. Clark, Rev. Mod. Phys. **66**, 539 (1994).
[10] C. Bahrim and U. Thumm, Phys. Rev. A **61**, 022722 (2000).
[11] K. Bartschat and H. R. Sadeghpour, J. Phys. B **36**, L9 (2003).
[12] D. H. Lee, W. D. Brandon, D. Hanstorp, and D. J. Pegg, Phys. Rev. A **53**, R633(R) (1996).
[13] M. Scheer, J. Thøgersen, R. C. Bilodeau, C. A. Brodie, H. K. Haugen, H. H. Andersen, P. Kristensen, and T. Andersen, Phys. Rev. Lett. **80**, 684 (1998).
[14] C. H. Greene, A. S. Dickinson, and H. R. Sadeghpour, Phys. Rev. Lett. **85**, 2458 (2000).
[15] A. A. Khuskivadze, M. I. Chibisov, and I. I. Fabrikant, Phys. Rev. A **66**, 042709 (2002).
[16] V. Bendkowsky, B. Butscher, J. Nipper, J. P. Shaffer, R. Löw, and T. Pfau, Nature (London) **458**, 1005 (2009).
[17] J. P. Shaffer, S. T. Rittenhouse, and H. R. Sadeghpour, Nat. Commun. **9**, 1965 (2018).
[18] C. Bahrim, U. Thumm, and I. I. Fabrikant, Phys. Rev. A **63**, 042710 (2001).
[19] F. Hummel, C. Fey, and P. Schmelcher, Phys. Rev. A **99**, 023401 (2019).
[20] S. T. Rittenhouse and H. R. Sadeghpour, Phys. Rev. Lett. **104**, 243002 (2010).
[21] M. T. Eiles and C. H. Greene, Phys. Rev. Lett. **115**, 193201 (2015).
[22] V. Bendkowsky, B. Butscher, J. Nipper, J. B. Balewski, J. P. Shaffer, R. Löw, T. Pfau, W. Li, J. Stanojevic, T. Pohl, and J. M. Rost, Phys. Rev. Lett. **105**, 163201 (2010).
[23] M. Jungen and V. Staemmler, J. Phys. B **21**, 463 (1988).
[24] E. L. Hamilton, C. H. Greene, and H. R. Sadeghpour, J. Phys. B **35**, L199 (2002).
[25] T. Niederprüm, O. Thomas, T. Eichert, C. Lippe, J. Pérez-Ríos, C. H. Greene, and H. Ott, Nat. Commun. **7**, 12820 (2016).
[26] M. T. Eiles and C. H. Greene, Phys. Rev. A **95**, 042515 (2017).
[27] S. Markson, S. T. Rittenhouse, R. Schmidt, J. Shaffer, and H. R. Sadeghpour, Chem. Phys. Chem. **17**, 3683 (2016).
[28] See Supplemental Material at http://link.aps.org/supplemental/10.1103/PhysRevLett.123.073003 for details on the excited dimer states, modeling and fitting of the scattering lengths, and calculation of PECs and line shapes, which includes Refs. [29–38].
[29] F. Hummel, C. Fey, and P. Schmelcher, Phys. Rev. A **97**, 043422 (2018).
[30] W. Li, I. Mourachko, M. W. Noel, and T. F. Gallagher, Phys. Rev. A **67**, 052502 (2003).
[31] J. Han, Y. Jamil, D. V. L. Norum, P. J. Tanner, and T. F. Gallagher, Phys. Rev. A **74**, 054502 (2006).
[32] J. E. Sansonetti, J. Phys. Chem. Ref. Data **35**, 301 (2006).

[33] E. Arimondo, M. Inguscio, and P. Violino, Rev. Mod. Phys. **49**, 31 (1977).
[34] L. Hostler and R. H. Pratt, Phys. Rev. Lett. **10**, 469 (1963).
[35] V. A. Davidkyn, B. A. Zon, N. L. Manakov, and L. P. Rapoport, Zh. Eksp. Teor. Fiz. **60**, 124 (1971) [Sov. Phys. JETP **33**, 70 (1971)].
[36] A. Omont, J. Phys. **38**, 1343 (1977).
[37] S. P. Andreev, B. M. Karnakov, V. D. Mur, and V. A. Polunin, Zh. Eksp. Teor. Fiz. **86**, 866 (1984) [Sov. Phys. JETP **59**, 506 (1984)].
[38] S. P. Andreev, B. M. Karnakov, and V. D. Mur, Theor. Math. Phys. **64**, 838 (1985).
[39] D. A. Anderson, S. A. Miller, and G. Raithel, Phys. Rev. A **90**, 062518 (2014).
[40] C. Fey, M. Kurz, P. Schmelcher, S. T. Rittenhouse, and H. R. Sadeghpour, New J. Phys. **17**, 055010 (2015).
[41] M. Deiß, S. Haze, J. Wolf, L. Wang, F. Meinert, C. Fey, F. Hummel, P. Schmelcher, and J. Hecker Denschlag, arXiv: 1901.08792.
[42] F. Böttcher, A. Gaj, K. M. Westphal, M. Schlagmüller, K. S. Kleinbach, R. Löw, T. C. Liebisch, T. Pfau, and S. Hofferberth, Phys. Rev. A **93**, 032512 (2016).
[43] R. G. Parsons and V. F. Weisskopf, Z. Phys. **202**, 492 (1967).
[44] In Ref. [22], the smaller value for the *p*-wave resonance position was concluded from spectroscopy of the weakly bound quantum reflection states, which are less sensitive to the resonance than the states *A* and *B*. Additionally, and in contrast to this work, an effective range approximation was employed to model the scattering length.
[45] I. I. Fabrikant, J. Phys. B **19**, 1527 (1986).
[46] M. T. Eiles, J. Pérez-Ríos, F. Robicheaux, and C. H. Greene, J. Phys. B **49**, 114005 (2016).
[47] C. Fey, J. Yang, S. T. Rittenhouse, F. Munkes, M. Baluktsian, P. Schmelcher, H. R. Sadeghpour, and J. P. Shaffer, Phys. Rev. Lett. **122**, 103001 (2019).
[48] M. Tarana and R. Čurík, Phys. Rev. A **99**, 012708 (2019).
[49] H. Hotop, M.-W. Ruf, M. Allan, and I. I. Fabrikant, Adv. At. Mol. Opt. Phys. **49**, 85 (2003).